In-flight calibration of the EOS/ Multi-angle Imaging SpectroRadiometer (MISR)

Carol J. Bruegge, Nadine C.L. Chrien, Brian G. Chafin, David J. Diner, Robert R. Ando

Jet Propulsion Laboratory, California Institute of Technology
4800 Oak Grove Dr., Pasadena, Ca. 91109

ABSTRACT

The Multi-angle Imaging SpectroRadiometer (MISR) is one of five instruments on the EOS/ Terra spacecraft. MISR consists of nine Earth-viewing cameras which continuously acquire global data sets in view perspectives from nadir to 70°. In order to maintain the radiometric calibration of the cameras, the instrument is equipped with an on-board calibrator. Spectralon panels, deployed at bi-monthly intervals, reflect sunlight into the cameras to be tested. This reflected light is measured by photodiode detectors which define the radiometric scale and allow the sensor calibration to be achieved. There exists six sets of four spectrally filtered photodiodes. For the first of the in-flight experiments the analysis was focused on validating the performance of the on-board calibrator components. As a result of these studies one blue-filtered, light-trapped detector was selected as the primary standard. All other on-board photodiodes have now been adjusted to be in agreement. This procedure has allowed improved band-to-band and camera-to-camera calibrations, in that all camera calibrations are traceable to a single standard. With these procedures in place MISR now plans to calibrate once every two months. New radiometric response coefficients will be delivered to the processing center following each experiment. This paper reports on these validation studies, and the post-launch radiometric response of the MISR cameras as determined during the first six months of on-orbit MISR calibration.

Keywords: on-orbit sensors, in-flight calibration

1. INTRODUCTION

The MISR instrument has been designed and built by the Jet Propulsion Laboratory (JPL). MISR's nine refractive cameras point nadir, forward, and aftward with respect to the spacecraft motion, and view at slant paths of 1.0, 1.1, 1.4, 2., and 3., as expressed by the inverse cosine of the view angles (i.e., 0.0°, 26.1°, 45.6°, 60.0°, and 70.5°). Global data sets are obtained for each of these views at four discrete spectral bands: 446, 558, 672, and 866 nm. Any given Earth location can be observed once every nine days at a minimum.

To achieve high quality scientific products, a radiometric accuracy specification of 3% absolute, 1 σ confidence level, was established at the project onset. Tolerances of 1% were given for the band- and camera-relative calibrations. During the assembly phase the cameras were extensively tested[1,2], both to assure that the design and build had produced the expected product, and to assess those sensor characteristics that could not be determined on-orbit. Results of these early studies were summarized into a database termed the Ancillary Radiometric Product (ARP)[3]. The ARP includes the band-dependent spectral response functions, an out-of-band correction matrix, band-weighted exo-atmospheric irradiances, point-spread function responses, and the camera radiometric coefficients. This file is used at the data processing center to produce geolocated and co-registered radiances (registered amongst the nine view angle and four spectral bands), aerosol optical depth and composition type, surface reflectance corrected for atmospheric effects, and other geophysical data products. To maintain MISRs radiometric accuracy, an equally ambitious post-launch program has been implemented. MISR has an on-board calibrator (OBC) which consists of two diffuse Spectralon reflectance panels and six sets of photodiode detector standards. Each of these sets contain four photodiodes filtered to the four MISR spectral bandpasses, thus there are 24 detectors monitoring the panels. Solar-reflected light from the panels, as measured by the photodiodes, regressed against the instrument output digital numbers (DN) determines the radiometric response of the instrument. Calibration experiments are done bi-monthly. The calibration sequence includes an observation of the dark-Earth side oceans, under new moon conditions. These data are used to monitor dark current stability.

On December 1999 MISR was launched as one of five instruments on the first Earth Observing System Terra platform[4]. On February 24, 2000, the outgassing phase was completed, and the cover was opened enabling the first views of the Earth. Within days the calibration panels were deployed for the first time, and now continue to be deployed once every two months. In addition to use of the OBC, Earth

views of desert targets allow an independent assessment of camera degradation. These desert studies are of two types. Vicarious calibration experiments are conducted at near-by desert regions, such as Lunar Lake, Nevada. For these experiments extensive measurements of the atmosphere and surface are made at the time of overpass. Because of their complexity, these experiments are conducted only twice a year. The second type of desert experiment is known as the Saharan desert study. Although, in principal, stable desert sites at any location on the globe could be used, the Saharan sites have been observed by a variety of satellites over a number of years, and have been reported to be extremely stable in surface reflectance[5,6]. Because no in-situ data are required for this methodology, more frequent observations are allowed as compared to the vicarious calibration experiments. Currently we are monitoring the stability of the MISR cameras (and photodiodes) using three Saharan sites each of which is observed, with a near-nadir view angle, once every 16 days. The validation of the MISR calibration using these desert studies will be the topic of future publications.

2. ON-BOARD CALIBRATOR

2.1 Experiment overview

A schematic of the MISR on-board calibrator (OBC) is shown in Figure 1. The diffuse panels are made from Spectralon, a material that has a high, near-Lambertian reflectance. While not in use the panels are stowed and protected by a labyrinth seal. At approximately bi-monthly time intervals the panels are deployed for calibration. The figure shows the nine MISR cameras, with the North Pole panel in its deployed position. That is, over the North Pole this plate will swing aftward to the position shown to diffusely reflect sunlight into the fields-of-view of the aftward-looking and nadir cameras. This figure also shows the South Pole panel in its stowed position. Over the South Pole this plate will swing forward for calibration of the forward-looking and nadir cameras. Because of data rate considerations, the nadir-camera views of the North Pole panel are used to calibrate only two of its four spectral channels (the Blue and Green bands); views of the South Pole panel are used to calibrate the nadir Red and NIR bands. Channels that are being tested are commanded into 275 m high-resolution mode; all others are placed in 4x4 pixel averaging mode to decrease the data rate. During use the panels are deployed to an angle of 67.5° with respect to the spacecraft plane, and receive solar illumination in a range from about 38° to 55° from the panel nadir.

Six sets of detector standards are used to monitor the radiance reflected from these panels, with each set consisting of four photodiodes filtered to the four MISR spectral passbands. The photodiodes are of three basic designs. As different designs may degrade at different rates, the diode that appears to have the greatest stability on-orbit can be used to establish the radiometric scale for the instrument. This standard may change with time, as one design may have greater near-term stability, another greater long-term stability. Five of the six photodiode sets consist of single photodiodes, termed PIN photodiodes. These are mounted at two nadir-viewing positions, at the Da and Df camera viewing positions, and on a goniometer which swings at ±65° along the flight direction. The PIN detectors have not been optimized for internal quantum efficiency, and therefore are of a more conventional design. The sixth photodiode set is nadir viewing, and is constructed in a light trap configuration using High Quantum Efficiency (HQE) photodiode technology. Two architecture types for the HQEs are utilized, one for the Blue, Green, and Red filtered photodiodes, and the second for the NIR filtered photodiode. The HQE diodes are designed to provide 100% external quantum efficiency, and thus have a response that can be determined to high accuracy using only knowledge of the area, field-of-view product, and the filter transmittance. In practice, all flight detectors have spectral out-of-band response levels greater than that predicted from a measurement of their filter transmittances[7]. For this reason all flight photodiode standards are calibrated by reference to the preflight laboratory detectors, rather than by using their component parameters.

During on-orbit calibration, data are acquired simultaneously with the photodiode detector standards, and the CCD cameras. This occurs throughout a five minute window, during which the sun transits a range of solar illumination and azimuth angles. A large range of illumination is desired during calibration, to gather data throughout the dynamic range of the sensor, and to test the camera linearity of the response as compared to that of the photodiodes. The varying solar angle onto the diffuse panel provides only minimal reduction in illumination during the experiment. Far greater attenuation is provided during the seconds where solar light is attenuated as it passes through the limb of the Earth's atmosphere. Figure 2 shows the measured camera output for the An-Red channel. These data were acquired during a calibration at the South Pole, April 29, 2000. The incident radiances correspond to a range in equivalent reflectance of 0. to 0.7. (The equivalent reflectance is a radiance, normalized by the solar-irradiance divided by pi, $\rho_{eq} = (L\pi)/E_0$. The cameras have 14-bit analog-to-digital conversion, and with the data compression scheme the DN saturation value is 16373. The minimum DN output is set by a bias signal which changes in response to the scene illumination but is typically on the order of 300 DN. This output is termed

the video bias, DN_0, and is measured once every line sample time. We see that the in-flight calibration experiment covers roughly 3/4 of the dynamic range of the sensor under test. This upper limit is determined by the smallest solar illumination angle onto the panel.

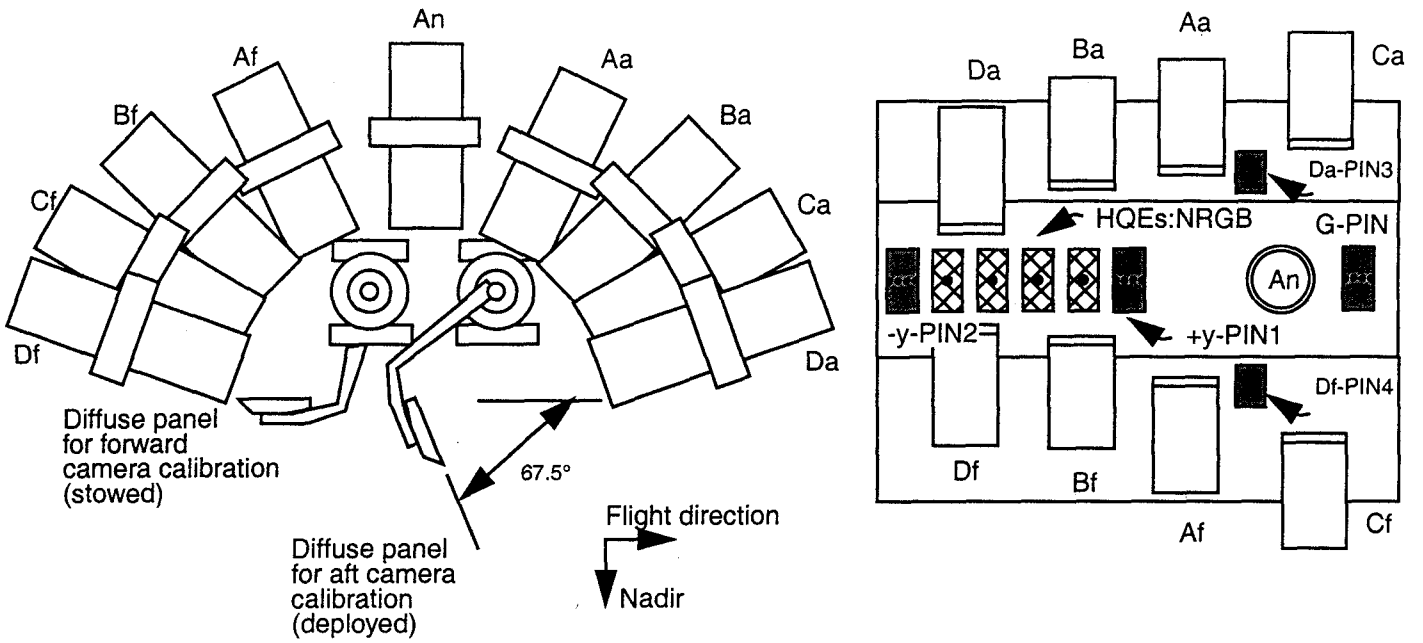

Figure 1. Schematic of MISR on-board calibrator. The deployed panels is termed the North Panel, as it is deployed over the North Pole; the panel in the stowed panel is called the South Panel.

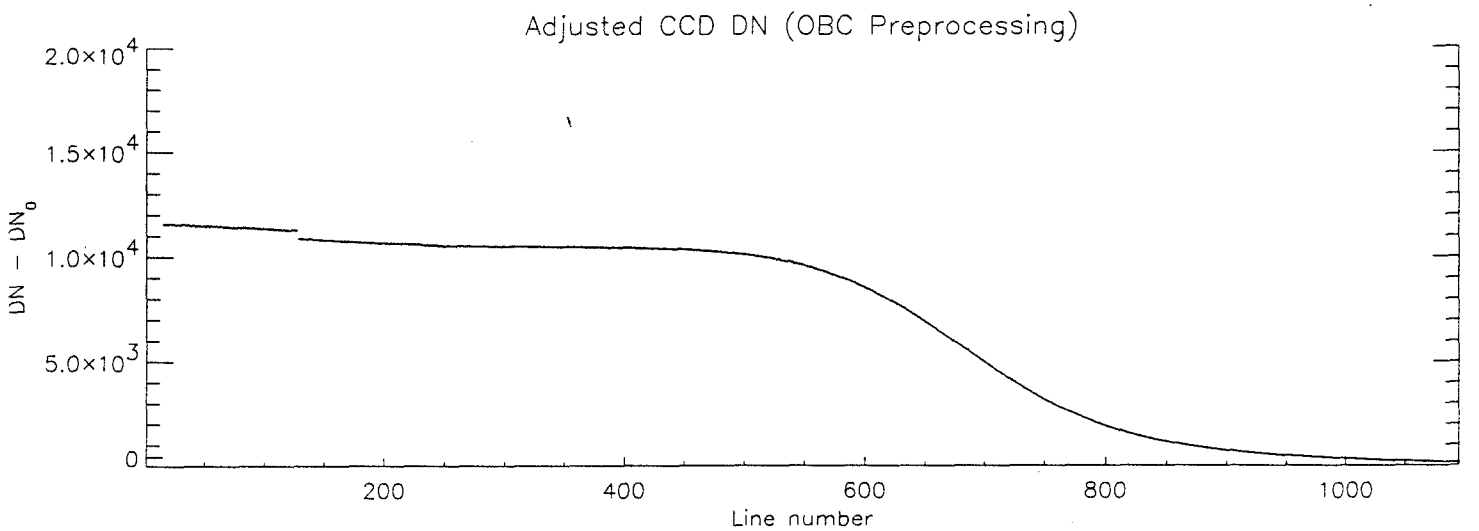

Figure 2. Measured camera digital number output for the An camera, Red Band, April 29, 2000. The peak incident signal was roughly 340 W m^{-2} sr^{-1} μm^{-1}, or about 0.7 in equivalent reflectance (radiance normalized by E_0/π).

2.2 Data reduction

The radiometric calibration of a given MISR channel is obtained when the camera-incident radiance, L, is regressed against the camera output DN. The calibration equation we elect to use for the reduction of data acquired on-orbit is linear in this relationship:

$$DN - DN_0 = LG_1 \tag{1}$$

Here G_1 is the gain coefficient to be determined from the experiment. The use of this equation is a change from preflight, where a quadratic equation was utilized in order to verify camera linearity. The reduction of on-orbit data using a quadratic equation may still be done on occasion, however as long as the cameras remain linear we prefer the simpler data analysis approach. In comparison of the preflight and post-launch equations, it is also noted that the offset coefficient G_0 has also been eliminated. We now place the physical constrain on the regression, knowing that the minimum digital count, by definition, is equal to the videobias term, DN_0, measured under dark illumination conditions.

The photodiodes have a field-of-view of 2.5°, and the cameras have a cross-track field of view as large as ±14.9° (for the A-designed lens). For this reason the photodiodes measure light in the same view geometry as the cameras for only a few center pixels within the A and D cameras. There are no stationary photodiodes in the B or C viewing angle directions, although the goniometer can swing through these angles. To provide a measure of radiance at each of the camera view angles, knowledge of the relative panel bidirectional reflectance function (BRF) is therefore required. This function is used to transfer measured diode radiances to the radiance that is reflected into a camera-view angle. BRF data were measured during preflight testing[8]. The transfer formula is determined by the relationship $L = (RE_0\cos\theta_0)/\pi$, where E_0 is the exo-atmospheric solar irradiance, R the panel bidirectional reflectance function (BRF), and θ_0 is the solar zenith angle onto the panel. Since the quantity $E_0\cos\theta_0$ is a property only of the incident light, we see that the radiance to BRF ratio is invariant for a given incident angle of illumination. Thus,

$$L^{ccd}(\theta_r^{ccd}, \phi_r^{ccd}) = L^{obc}(\theta_r^{obc}, \phi_r^{obc}) \cdot \frac{R(\theta_o;\theta_r^{ccd}, \phi_r^{ccd})}{R(\theta_o;\theta_r^{obc}, \phi_r^{obc})} \tag{2}$$

Here L^{obc} and L^{ccd} are radiances (weighted over the MISR spectral response functions) incident onto the OBC photodiodes and CCD pixels, respectively.

Using the new calibration equation, Eqn. 1, and constraining the regression equation to go through DN_0 in the limit of no incident radiance, an on-orbit determination of the response of each MISR pixel can be obtained.

2.3 Image quality assessment

During the month following the cover open four calibration experiments were conducted. The first calibration results were normalized to have the same channel-average G_1 as preflight. This was done to make use of the diffuse panel as a flat-field source, but to not yet utilize the photodiode standards. The results are depicted in Figure 3 for two of the 36 MISR channels. The plots shown are of the nadir and one of the two cameras which view at 26.1° for the Red Band, and are normalized to the preflight coefficients. The Af plot is also representative of the Aa camera, and the An is representative of the other seven cameras.

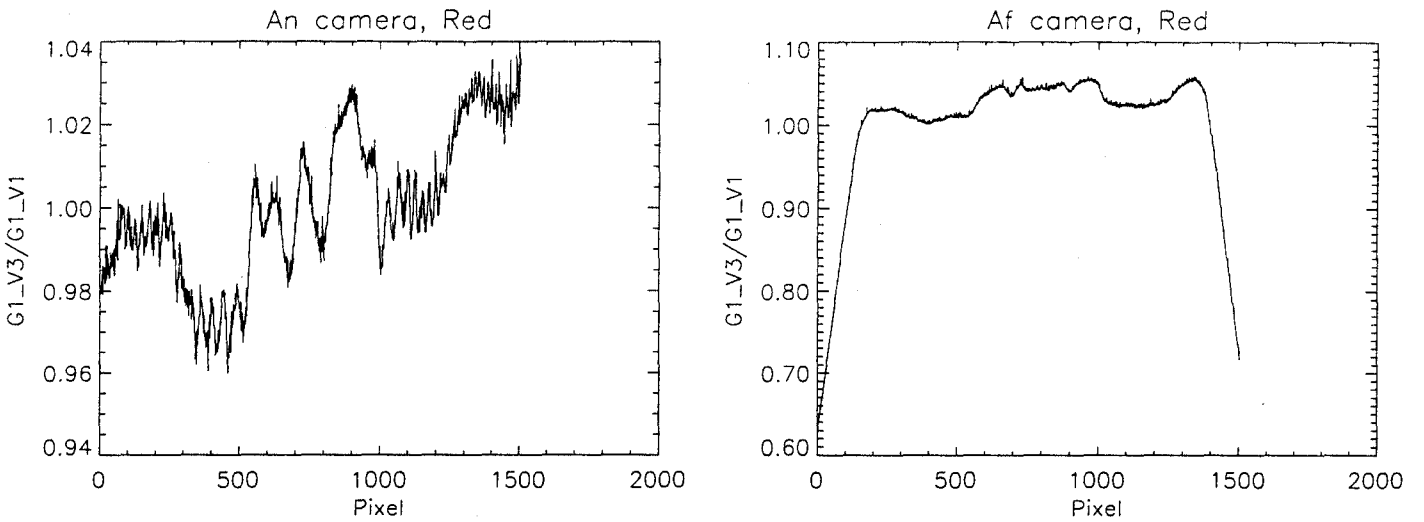

Figure 3. Normalized response coefficients for first post-launch OBC calibration: An and Af Red Channels.

The most apparent difference between the in-flight calibration and preflight is found in the Af and Aa view angles. For the edge 75 pixels, it is shown that the response drops by nearly 40%. This is observed only for these two cameras. This vignetting results from an obstruction which is present when the cameras are mounted to the instrument optical bench. The cameras did not view this obstruction when tested preflight, as each camera was tested as a stand-alone unit. The obstruction is due to undersized apertures within the optical bench. This manufacture error was observed preflight during instrument-level testing, but not considered critical. The vignetting can be corrected for in the calibration process, as has been observed in images generated using the newer coefficients.

A second artifact noticed in early data, processed using the preflight coefficient file, is striping in the imagery. Although radiometrically very small (a 1% effect), this stripping is particularly apparent over dark ocean, or other uniform targets when the image display stretch is magnified to bring out small features of an otherwise uniform target. To understand the nature of this feature, it is recalled that the coherence length of light is inversely proportional to its bandwidth, and given by the equation

$$\Delta x = \frac{c}{\Delta \upsilon} = \frac{\lambda^2}{\Delta \lambda} \tag{3}$$

Table 1 shows the coherence length for each of the MISR bands, assuming the bandwidths as computed by a moments analysis (i.e., the area equivalent square band)

Table 1. Coherence length for the four MISR spectral bands

MISR parameter	Band			
	1) Blue	2) Green	3) Red	4) NIR
λ, nm	446	558	672	866
$\Delta\lambda$, nm	25 (minimum equivalent squareband assumed)			
Δx, μm	8	12	18	30

It is known that any two incoherent wavefronts of common origin can interfere, provided they have not travelled a distance greater than their coherence length since their paths diverged. The interference pattern created due to their interference is given by the equation

$$E^2 = E_1^2 + E_2^2 + 2E_1E_2\cos(\delta) \quad (4)$$

where δ is the optical path difference. This peak amplitude is found when

$$\delta = \frac{2\pi}{\lambda} n\Delta d = 0, \pm n2\pi \quad (5)$$

In comparing the coherence length, Table 1, to the schematic of the MISR focal plane, Figure 4, we see that there are multiple surfaces in which a beam could be reflected. However, the structures which are in closest proximity are the glass plates which are coated respectively with the interference and blocking coating layers. These surfaces are the most probable location where interference could arise. We note from observations of imagery produced using the preflight coefficients that the fringing spacing is greatest at the center of the image. This is consistent with the filter stack having a greater separation in the center, as could happen if the filter stack were secured at its edges, and allowed to bow in the center, where it is unconstrained (note this separation difference only need be a fraction of a wavelength to be observable in the fringes).

When the post-launch coefficients are applied to this same image, the interference fringing is no longer visible. One explanation is that the launch vibration slightly changed this separation. Once in-orbit, however, the focal plane becomes stable, and any interference effects are able to be removed with the on-orbit calibration.

2.4 Verifying the calibrator

The first post-launch ARP calibration file maintained the channel-average coefficients, as determined preflight. This was done in that there was hesitation in basing a calibration on the OBC, prior to verification of its components. Nevertheless, as shown in the previous section, there was benefit to releasing a new file and allowing vignetting and interference fringing to be removed.

The second step is to validate the OBC, for example by comparison of photodiode measured radiances to those predicted from independent means. This is easily done, in that the exo-atmospheric solar irradiance can be modeled, and in that the diffuse panel BRF was measured preflight. Figure 5 shows this comparison of measured versus predicted photodiode radiance, using the preflight calibration of the OBC photodiodes. It is apparent that there is an offset bias in the predicted versus measured radiances, particularly for the PIN photodiodes. We now believe this is a consequence to the preflight photodiode calibration methodology, which may not have accounted for spectral out-of-band response. It is noted that the HQE photodiode assemblies have better out-of-band rejection, and this may explain their improved agreement with the predicted radiances, as compared to the PIN photodiodes. The last column in these plots shows a comparison of the HQE NIR response to predicted, in which an attempt was made to redo the preflight calibration, and account for the out-of-band response. The fact that there is better agreement with the predicted again supports our hypothesis as to the nature of the erroneous calibrations.

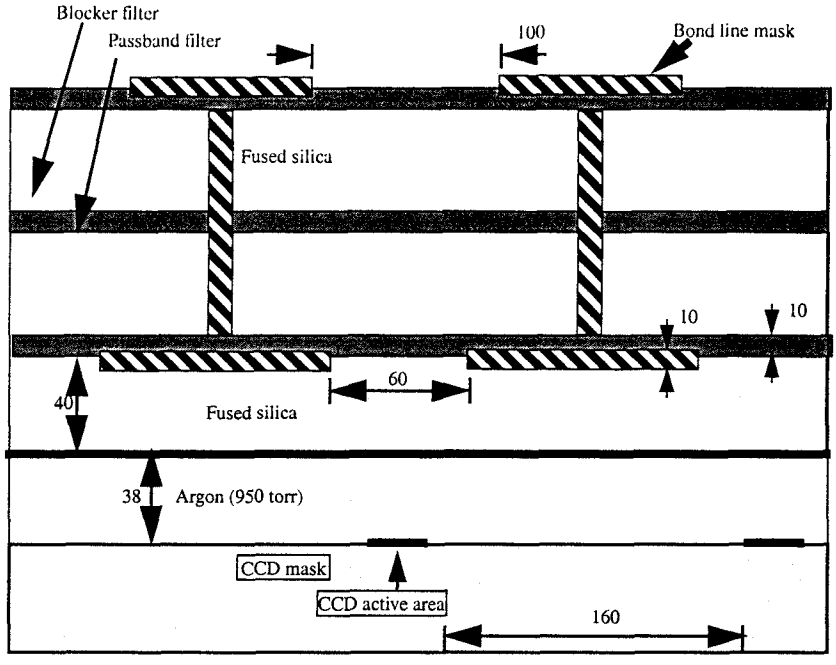

Figure 4. MISR focal plane schematic

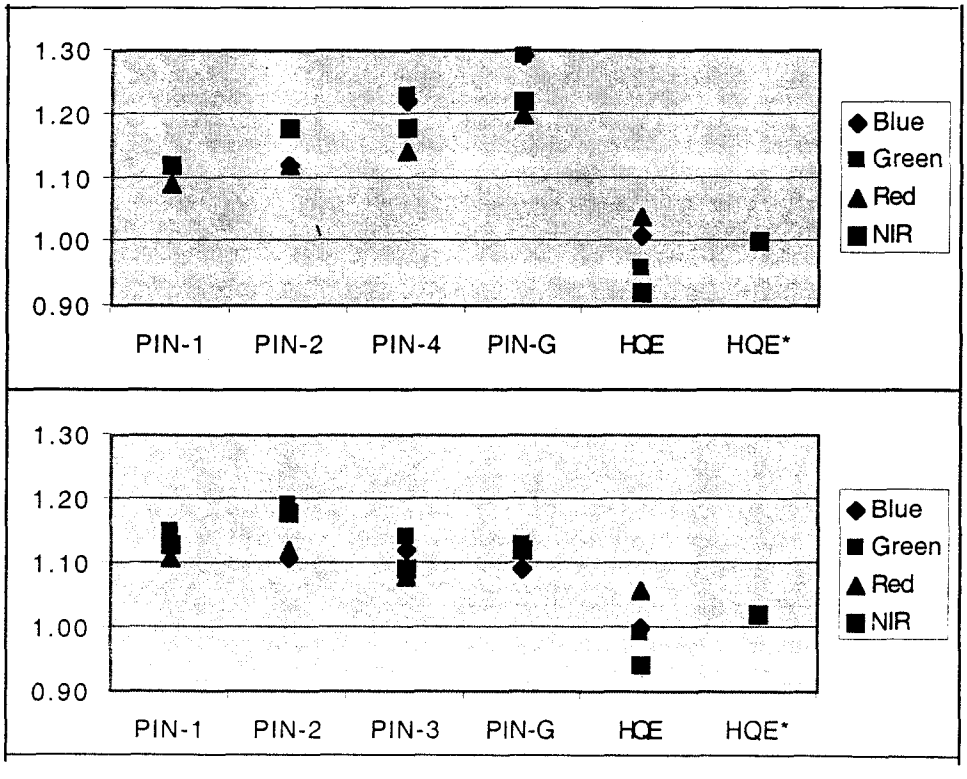

Figure 5. Predicted versus measured photodiode response. Upper figure is for March 13, 2000, orbit 1259 (Cal-North); lower figure is for April 27, 2000, orbit 1912 (Cal-South).

This study led us to conclude that the OBC photodiodes needed to be recalibrated on-orbit. The method to do this was to assume one photodiode to be correct (the HQE Blue), and to adjust all photodiode responses accordingly. This was done by taking the ratio of photodiode currents, during observations of the diffuse panel. The photodiode calibration constants were adjusted until they predicted these measured current ratios. This algorithm is developed in the following paragraphs.

The photodiode response functions include a product of the diode étendue, the diode integrated solar-weighted spectral response, and the diode calibration correction factors. The diode integrated solar-weighted spectral response is defined in Eqn. 6, where $E_{0,\lambda}$ is the exo-atmospheric solar irradiance and R_λ is the diode spectral response.

$$\Re = \int_{200nm}^{1200nm} E_{0,\lambda} R_\lambda \lambda d\lambda \tag{6}$$

The diode étendue, AΩ, is the area times projected solid angle product for the photodiode.The diode calibration correction factors are multiplicative factors that are applied to the product of the diode AΩ and the diode integrated solar-weighted spectral response. The preflight calibration of the blue HQE diode is used as the standard to which the other photodiodes are calibrated. The D-diodes are calibrated using the goniometer to provide a transfer calibration. The OBC data collected during orbits 1259 and 1912 for Cal-North and Cal-South respectively were used for this first adjustment. The calibration correction factors represent the average correction factor computed for Cal-North and Cal-South with the exception of the D-diode factors. For the D-diode factors, the north-south average is applied to the PIN-G for the transfer, but PIN-3 only views the south panel and PIN-4 only views the north panel.

The radiance measured by a given photodiode is computed following Eqn. 7 where k is the calibration correction factor. The calibration correction factor is computed based upon the assumption that the Spectralon® calibration panels are spectrally neutral in reflectance. This implies that the ratio of one diode current to another should equal the ratio of étendue-response products, AΩℜ (Eqn. 8). The calibration correction factors for the nadir viewing diodes are computed using the blue HQE diode and its preflight calibration as the standard, i.e., $k_{\text{HQE, blue}} = 1$ (Eqn. 9). The D-diodes, PIN-3 and PIN-4, are calibrated to the blue HQE diode using the goniometer, PIN-G, as a transfer standard. The goniometer calibration correction factor is computed using currents when the goniometer position is nadir-viewing. The D-diode bands are then calibrated to the goniometer diode bands as shown in Eqn. 10.

$$L^{\text{std, OBC}} = \frac{1.2395 i E_0^{std}}{(A\Omega\Re)\cdot k} \tag{7}$$

$$\left[\frac{i_2}{(A\Omega\Re)_2 \cdot k_2} = \frac{L_2^{\text{std,OBC}}}{E_{0,2}^{std}} = \frac{L_1^{\text{std,OBC}}}{E_{0,1}^{std}} = \frac{i_1}{(A\Omega\Re)_1 \cdot k_1}\right] \Rightarrow \left(\frac{i_2}{i_1} = \frac{(A\Omega\Re)_2}{(A\Omega\Re)_1} \cdot \frac{k_2}{k_1}\right) \tag{8}$$

$$k_{\text{diode, band}} = \frac{i_{\text{diode, band}}}{i_{\text{HQE, blue}}} \div \frac{(A\Omega\Re)_{\text{diode, band}}}{(A\Omega\Re)_{\text{HQE, blue}}} \tag{9}$$

$$k_{\text{D-diode,band}} = \frac{i_{\text{D-diode,band}}}{i_{\text{goni, band @D-angle}}} \div \frac{(A\Omega\Re)_{\text{D-diode,band}}}{(A\Omega\Re)_{\text{goni, band}} \cdot k_{\text{goni, band}}} \tag{10}$$

Using this new approach, the OBC photodiodes were recalibrated, then these photodiodes were used to calibrate the MISR cameras. Table 2 gives the resulting channel averages for the April 27, 2000 calibration. We have posted these results to the Version 4 ARP. Here the radiances based upon the preflight calibration used a laboratory integrating sphere as flat-field source. We call these coefficients Version 1; the first which were based upon the flight panel (but having the same preflight channel mean) are called Version 3.

To convert radiances whose gain coefficients are based on the first two calibraiton files to radiances which are based upon the OBC determination described here, one would multiply by the constants in Table 3.This algorithm has been deduced from Eqn. 1, and the relationship

Table 2. Version 4 G1 coefficient, channel mean: ($G_{1,v4}$)

Camera	Band			
	Blue	Green	Red	NIR
Df	25.1400	24.5340	29.1016	47.2038
Cf	23.1820	23.6575	31.2472	48.4285
Bf	23.2045	21.7657	28.8087	46.2912
Af	23.4616	23.7062	29.2541	45.7679
An	22.5434	22.9652	30.7784	45.4112
Aa	22.4853	24.1517	27.5552	43.3149
Ba	24.8146	24.2892	26.5047	49.3487
Ca	23.2513	21.8879	27.0821	45.3921
Da	22.7255	21.2316	25.6618	42.1603

Table 3. Factors to convert from ARP version 3 radiances to version 4 radiances, $\frac{G_{1,v3}}{G_{1,v4}}$

Camera	Band			
	Blue	Green	Red	NIR
Df	0.9440	0.9579	0.9649	0.9347
Cf	1.0010	1.0164	0.9445	0.9287
Bf	1.0204	1.0401	1.0223	0.9872
Af	0.9987	0.9962	1.0001	0.9574
An	0.9284	0.9553	0.9812	0.9624
Aa	1.0309	1.0069	1.0495	0.9860
Ba	1.0501	0.9797	1.0392	0.9698
Ca	0.9905	1.0553	1.0309	0.9844
Da	1.0159	1.0714	1.0699	1.0057

$$L_{v4} = L_{v3} \cdot \frac{G_{1,v3}}{G_{1,v4}} \tag{11}$$

This study has been continued for a range of dates. It is apparent that the green and nir channels are drifting as compared to their predicted response. Because the blue HQE photodiode appears both to agree with its predicted radiance, and because this agreement has remained stable in time, we have elected to re-calibrate all the photodiode responses against this standard. This new procedure will be followed prior to the reduction of any future OBC calibration data sets.

3. CONCLUSIONS

One preflight, and two post-launch radiometric calibrations of MISR have been conducted to date. A summary of the differences between the resulting data files is summarized in Table 4. Bimonthly coefficient files will continue to be published, so as to allow any change in the MISR cameras to be tracked with time, and to allow data product computations to be made using this updated instrument response terms.

Table 4. A comparison of three ARP calibration coefficient files, released to date.

Comparison basis	Version 1	Version 3[a]	Version 4
Date first used in DAAC production	At-launch	June 1, 2000	August 1, 2000
Basis for radiometric scale	Laboratory HQEs (trapped photodiodes)	Preflight channel average	On-orbit HQE blue photodiode
Calibration equation	Quadratic, unconstrained intercept (G_0, G_1, and G_2 coefficients determined)	Linear, constrained intercept (G_0 coefficient constrained to zero)	Linear, constrained intercept
Vignetting correction	None, problematic for Aa, Af	Corrected using flight panel flat-field response	Corrected using flight panel flat-field response
Fringing	Apparent at 1% level	Corrected using flight panel flat-field response	Corrected using flight panel flat-field response
Uncertainties	Based upon preflight error analysis	Same as Ver1	Systematic errors doubled
Camera-to-camera and band-to-band relative calibrations	Uncertain to 5%	Uncertain to 5%	Improved by recalibrating all photodiodes to HQE-blue standard

a. Version 2 was reserved as the name for a reformated Version 1 file.

4. ACKNOWLEDGMENTS

The work described in this paper has been carried out by the Jet Propulsion Laboratory, California Institute of Technology, under contract with the National Aeronautics and Space Administration.

5. REFERENCES

1. Bruegge, C.J., V.G. Duval, N.L. Chrien, R.P. Korechoff, B.J. Gaitley, and E.B. Hochberg (1998). MISR prelaunch instrument calibration and characterization results. IEEE Trans. Geosci. Rem. Sens., Vol. **36**, pp. 1186-1198.

2. Bruegge, C.J., N. L. Chrien, R. A. Kahn, J. V. Martonchik, David Diner (1998). MISR radiometric uncertainty analyses and their utilization within geophysical retrievals. Conference issue: New Developments and Applications in Optical Radiometry (NEWRAD 1997), Metrologia, **35**, pp. 571-579.

3. Woodhouse, Robert M., Carol J. Bruegge, Barbara J. Gaitley, Ghobad Saghri, and Nadine L. Chrien (1997). Multi-angle SpectroRadiometer (MISR) Ancillary Radiometric Product. In Earth Observing System II, SPIE Vol. **3117**, San Diego, CA, pp. 158-169.

4. Diner, D.J., J.C. Beckert, T.H. Reilly, C.J. Bruegge, J.E. Conel, R. Kahn, J.V. Martonchik, T.P. Ackerman, R. Davies, S.A.W. Gerstl, H.R. Gordon, J-P. Muller, R. Myneni, R.J. Sellers, B. Pinty, and M.M. Verstraete (1998). Multiangle Imaging SpectroRadiometer (MISR) description and experiment overview. IEEE Trans. Geosci. Rem. Sens., Vol. **36**, pp. 1072-1087.

5. Cosnefroy, Helene., X. Briottet, M. Leroy (1993). Characterization of desert areas with Meteosat-4 data for the calibration of optical satellite sensors. In Recent Advances in Sensors, Radiometric Calibration, and Processing of Remotely Sensed Data, SPIE Vol. **1938,** Orlando, Florida, pp. 203-211.

6. Cabot, F., O. Hagolle, C. Ruffel, and Patrice Henry (1999). Use of a remote sensing data repository for in-flight calibration of optical sensors over terrestrial targets. In Earth Observing Systems II, SPIE Vol. **3750**, Denver, Colorado, pp. 514-523.

7. Korechoff, R.P, D.J. Diner, D.J. Preston, C.J. Bruegge (1995). In Advanced and Next-Generation Satellites. Spectroradiometer focal-plane design considerations: lessons learned from MISR camera testing. In Advanced and Next-Generation Satellites, EUROPTO/ SPIE Vol. **2538**, Paris, France, pp. 104-116.

8. Bruegge, Carol, Nadine Chrien, and David Haner (1999). A Spectralon BRF data base for MISR calibration applications. Accepted to Remote Sens. Environment.